

See discussions, stats, and author profiles for this publication at: <https://www.researchgate.net/publication/261837123>

Protein Coronas on Gold Nanorods Passivated with Amphiphilic Ligands Affect Cytotoxicity and Cellular Response to Penicillin/Streptomycin

ARTICLE *in* ACS NANO · APRIL 2014

Impact Factor: 12.88 · DOI: 10.1021/nn5002886 · Source: PubMed

CITATIONS

13

READS

142

8 AUTHORS, INCLUDING:



James Kah

National University of Singapore

28 PUBLICATIONS 429 CITATIONS

[SEE PROFILE](#)



Christin Grabinski

Wright-Patterson Air Force Base

16 PUBLICATIONS 368 CITATIONS

[SEE PROFILE](#)



Saber M Hussain

Wright-Patterson Air Force Base

137 PUBLICATIONS 8,081 CITATIONS

[SEE PROFILE](#)



Kimberly Hamad-Schifferli

University of Massachusetts Boston

53 PUBLICATIONS 2,263 CITATIONS

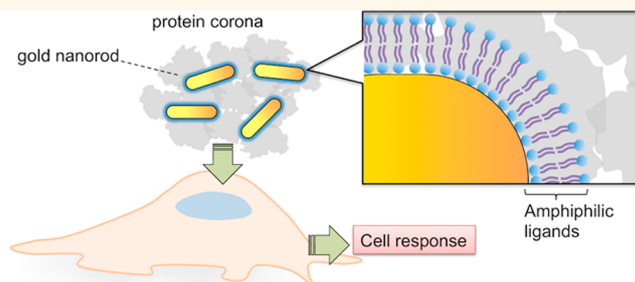
[SEE PROFILE](#)

Protein Coronas on Gold Nanorods Passivated with Amphiphilic Ligands Affect Cytotoxicity and Cellular Response to Penicillin/Streptomycin

James Chen Yong Kah,^{†,II} Christin Grabinski,[§] Emily Untener,[§] Carol Garrett,[§] John Chen,[†] David Zhu,[‡] Saber M. Hussain,^{§,*} and Kimberly Hamad-Schifferli^{†,‡,*,†,✉}

[†]Department of Biological Engineering and [‡]Department of Mechanical Engineering, Massachusetts Institute of Technology, 77 Massachusetts Avenue, Cambridge, Massachusetts 02139, United States and [§]Molecular Bioeffects Branch, Human Effectiveness Directorate, Air Force Research Laboratory, Wright-Patterson AFB, Dayton, Ohio 45433, United States. [✉]Present address: MIT Lincoln Laboratory, 244 Wood St., Lexington, MA 02420. ^{II}Present address: Nanomedicine & Nanobiology Lab, Department of Biomedical Engineering, National University of Singapore, Singapore 117575.

ABSTRACT We probe how amphiphilic ligands (ALs) of four different types affect the formation of protein coronas on gold nanorods (NRs) and their impact on cellular response. NRs coated with cetyltrimethylammonium bromide were ligand exchanged with polyoxyethylene[10]cetyl ether, oligofectamine, and phosphatidylserine (PS). Protein coronas from equine serum (ES) were formed on these NR-ALs, and their colloidal stability, as well as cell uptake, proliferation, oxidative stress, and gene expression, were examined. We find that the protein corona that forms and its colloidal stability are affected by AL type and that the cellular response to these NR-AL-coronas (NR-AL-ES) is both ligand and corona dependent. We also find that the presence of common cell culture supplement penicillin/streptomycin can impact the colloidal stability and cellular response of NR-AL and NR-AL-ES, showing that the cell response is not necessarily inert to pen/strep when in the presence of nanoparticles. Although the protein corona is what the cells see, the underlying surface ligands evidently play an important role in shaping and defining the physical characteristics of the corona, which ultimately impacts the cellular response. Further, the results of this study suggest that the cellular behavior toward NR-AL is mediated by not only the type of AL and the protein corona it forms but also its resulting colloidal stability and interaction with cell culture supplements.



KEYWORDS: gold nanorods · amphiphilic ligands · protein corona · cytotoxicity · nanotoxicology · penicillin · streptomycin

When nanoparticles (NPs) are introduced to biological fluids and cellular environments, the proteins and other species that are present at high concentration adsorb to their surface. This results in the formation of a protein corona, a multilayered cloud of proteins held together by weak noncovalent bonds. Although the properties of protein coronas are still being elucidated, it is clear that they have a significant biological impact on the fate of the NPs. Previous studies have shown that the physical characteristics of NPs such as size, material, surface chemistry, and charge influence the adsorption and binding of proteins on the NP.^{1–4} The NP properties alter the interactions with the adsorbed

proteins and, hence, the properties of the protein corona that forms.^{5–7} Protein coronas can, in turn, result in decreased specificity in targeting,^{8,9} altered biodistribution,^{10,11} and reduced cytotoxicity.^{12–14} Some studies have shown that formation of and changes in the protein corona dictated by different types of cell media can affect cellular uptake, where the presence of a protein coating correlated with lower uptake.^{15–17}

Because the molecules that passivate the NP surface are at the very center of the nanomaterial–biological interface, corona formation greatly depends on NP surface chemistry. However, the majority of studies on NP-coronae have focused primarily on NPs with covalently attached ligands^{1,4,18–21} or no

* Address correspondence to schiffer@mit.edu, saber.hussain@us.af.mil.

Received for review January 16, 2014 and accepted April 10, 2014.

Published online
10.1021/nn5002886

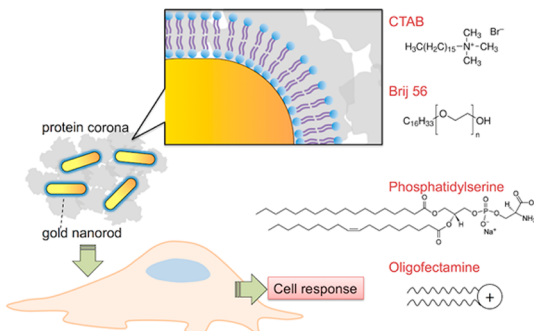
© XXXX American Chemical Society

ligands at all.^{13–15} One important class of ligands that has not been as well studied in corona formation is amphiphilic ligands (ALs). ALs have been used extensively in delivery applications because of their ability to form micelles and liposomes that have high capacity for payloads of small molecule drugs, DNA and siRNA.^{22–25} Since ALs are similar to the cell membrane, they can reduce cytotoxicity²⁶ and fuse with the endosomal membrane during uptake, enabling cytoplasmic delivery.^{23,24,27} The properties of ALs and their ability to passivate NPs are unique from covalently bound ligands because, unlike covalently attached ligands, ALs on the NP surface exchange with free ALs. Free ALs can also interact with the proteins in the environment and in the corona, so the interactions in a corona are expected to be highly complex, involving the NP, bound ligand, free ligand, and the surrounding proteins. Some common ALs such as cetyltrimethylammonium bromide (CTAB) included in the present study have been proven to be cytotoxic, especially in their free form.^{28,29} Therefore, properties of coronas on NPs coated with ALs and their impact on cellular response needs to be understood.

Here we probe how ALs of different types affect formation of protein coronas on gold nanorods (NRs) and consequently their impact on cellular response. We chose to study NRs because of their unique optical properties that allow a wide range of biological applications, including biosensing, imaging, laser triggered release, and numerous other applications in theranostics.^{30,31} We passivate NRs with four ALs of different headgroup charges (NR-ALs): the as-synthesized NRs stabilized with CTAB, NRs stabilized with neutrally charged surfactant polyoxyethylene[10]cetyl ether (Brij56), NRs passivated with the cationic phospholipid oligofectamine (OF), and the anionic lipid phosphatidylserine (PS). We form protein coronas on the NR-ALs from equine serum (ES) and assess colloidal stability, cell uptake, proliferation, oxidative stress, and gene expression (Scheme 1). We find that the protein corona that forms and its colloidal stability is affected by AL type and that the cellular response to these NR-AL-coronas (NR-AL-ES) is both ligand and corona dependent. We also find that the presence of the common cell culture supplement penicillin/streptomycin (pen/strep) can impact the colloidal stability and cellular response of NR-AL and NR-AL-ES, which is most likely due to the high capacity of the ALs and protein coronas for small molecules. The results suggest that the cellular behavior toward NR-AL is mediated by the surface ligand, the protein corona it recruits, and its resulting colloidal stability and interaction with cell culture supplements.

RESULTS AND DISCUSSION

Ligand Exchange and Serum Protein Adsorption on NR-AL. NRs with dimensions of 42.9 ± 4.1 nm by 11.4 ± 1.4 nm



Scheme 1. Effect of corona formation on cellular response for NRs passivated with different ALs.

(aspect ratio = 3.6) and a longitudinal surface plasmon resonance (LSPR) at 800 nm were synthesized and chosen as the scaffold for corona formation. Ligand exchange was performed on CTAB-passivated NRs (NR-CTAB) using competitive place exchange with other ALs²³ to form a set of NR-ALs with different surface charges. TEM imaging of the NR-ALs showed that ligand exchange did not affect the NR morphology (Figure 1a). Ligand exchange was probed by zeta-potential and gel electrophoresis (Figure 1b). The zeta-potential of NR-CTAB (+43.4 mV) changed to +35.6 mV when the ligand was changed to OF, which is positively charged. Ligand exchange to Brij56 resulted in a zeta-potential of +4.9 mV, suggesting that the neutral Brij56 mostly replaced the CTAB. Exchange to the negatively charged PS resulted in a zeta-potential of –47.0 mV.

Gel electrophoresis, which probes both the size and charge of a species simultaneously, showed shifts toward the negative electrode for the NR-OF and positive electrode for the NR-PS. NR-Brij56 stayed near the well, suggesting a neutral species. NR-CTAB did not run from the well as they aggregated in buffer. Thus, zeta-potential and gel electrophoresis suggest successful ligand exchange. The NRs with the different ALs had different values for their average D_H (Figure 1c), showing that the ALs passivate the NRs to different extents, resulting in different levels of aggregation and thus a population spread with different sizes. It is important to note that the ALs can form micelles and other structures that can range from ~1 nm to 100s of nanometers in size, which can impact the measured average D_H .

We formed protein coronas around NR-ALs using 0.4% ES by volume based on the colloidal stability it confers. Our previous experiments have shown that 0.4% ES is not just able to confer good colloidal stability to the NRs but also allow small molecule drugs to be loaded on them as a drug delivery vehicle.^{32,33} This study serves to extend our previously published work by evaluating the cellular response of the NR-ES delivery vehicle. The zeta-potential became negative with corona formation as the serum proteins are negatively charged (Figure 1b). Gel electrophoretic mobility showed

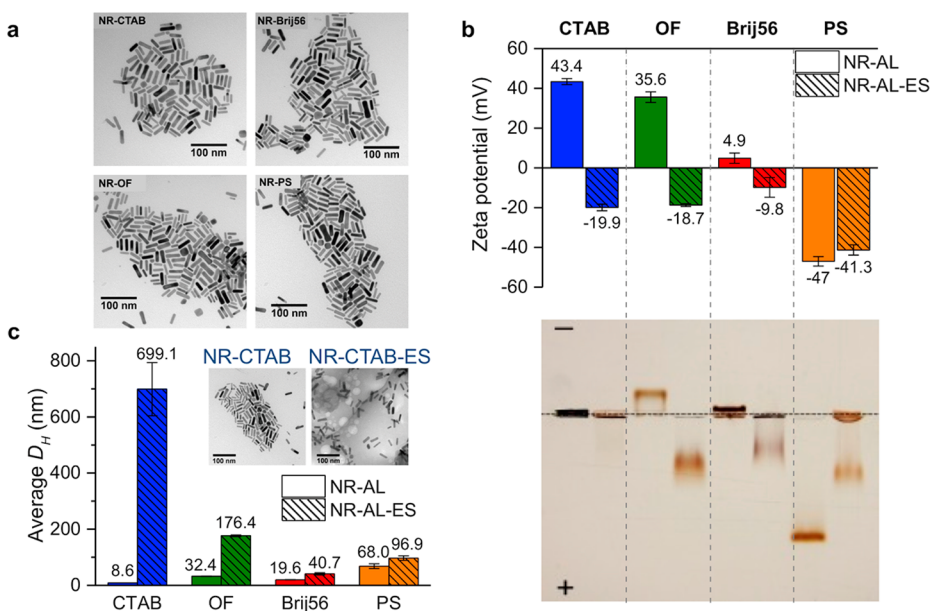


Figure 1. Characterization of various NR-AL and NR-AL-ES in this study: (a) TEM; (b) zeta potentials (top) and agarose gel electrophoresis (0.2%) (bottom), with each lane corresponding to the samples as indicated in the zeta potential plot; and (c) average D_H measured by DLS. Inset: TEM of NR-CTAB and NR-CTAB-ES. Error bars indicate standard deviation.

increases toward higher negative mobility for all the NR-ALs except NR-CTAB, suggesting corona formation. Despite having a negative charge, NR-CTAB-ES did not migrate out of the well, probably due to its large average hydrodynamic diameter, D_H , and tendency to precipitate in buffer. The NR-PS-ES band was shifted to lower mobility relative to NR-PS. Since the zeta-potential of NR-PS did not change appreciably upon corona formation, its band shift is most likely due to an increase in size upon corona formation, as gel electrophoretic mobility is due to both size and charge.

Corona formation was confirmed by increases in D_H (Figure 1c). The large ΔD_H observed for the positively charged NR-CTAB-ES and NR-OF-ES (690.5 and 144.0 nm, respectively) supports the formation of large agglomerates containing several NRs, which is most likely due to strong charge interactions between the positive ALs and serum proteins. TEM imaging showed the NRs embedded in a diffuse cloud of proteins (Figure 1c, inset). NR-Brij56 and NR-PS exhibited smaller ΔD_H upon corona formation (21.1 and 28.9 nm, respectively), suggesting that a less extensive corona was formed. This was most likely due to the reduced interaction from charge repulsion. These results show that the surface charge can influence the extent of corona formation, although we note that our observations differ from that of Huhn *et al.*, who observed that the charge on NPs did not have any influence on the number of adsorbed human serum albumin (HSA) molecules.³⁴ This could be attributed to the fact that we used the full equine serum comprising of >3000 proteins, in contrast to Huhn *et al.*, who study the interaction with only human serum albumin. The whole suite of proteins in the serum could have caused the

corona to form differently with more dependence on charge compared to a single protein.

Colloidal Stability with Corona Formation. We examined the colloidal stability of the NRs with the different ALs and preformed coronas using an aggregation index (AI) that was previously developed.³⁵ The AI is based on the LSPR shift and broadening, and a higher AI indicates higher aggregation. The AI for all four NR-ALs were approximately the same in nonionic water (Figure 2a, solid bars), suggesting similar colloidal stability. Upon corona formation, there was a more pronounced AI increase for the positively charged ALs (NR-CTAB-ES and NR-OF-ES) while there was no change in NR-Brij56 and NR-PS. This increase in AI also confirms NR clustering and that the nature of the AL affects the colloidal stability of the NR-AL-ES.

When NR-ALs were put into RPMI cell culture media, their colloidal stability changed (Figure 2b, solid bars). While most NR-ALs remained stable in cell culture media, as evidenced by little or no change in AI, the AI of NR-CTAB increased (159 to 213 nm), suggesting aggregation (Figure 2b, blue solid bar). NR-ALs with preformed coronas of ES were more stable, showing that the corona stabilizes the NR-ALs against aggregation for all ALs in cell culture media (Figure 2b, hatched bars), although with smaller improvements for OF and PS. The improvement in colloidal stability with protein corona formation has been reported elsewhere.^{36,37} This improvement of NR-AL-ES stability in biological media could potentially affect how the cells see the NR-ALs and respond to them.

Influence of AL and Corona Formation on Cell Uptake. We evaluated the cellular response by first examining the uptake of NR-AL and NR-AL-ES in the human

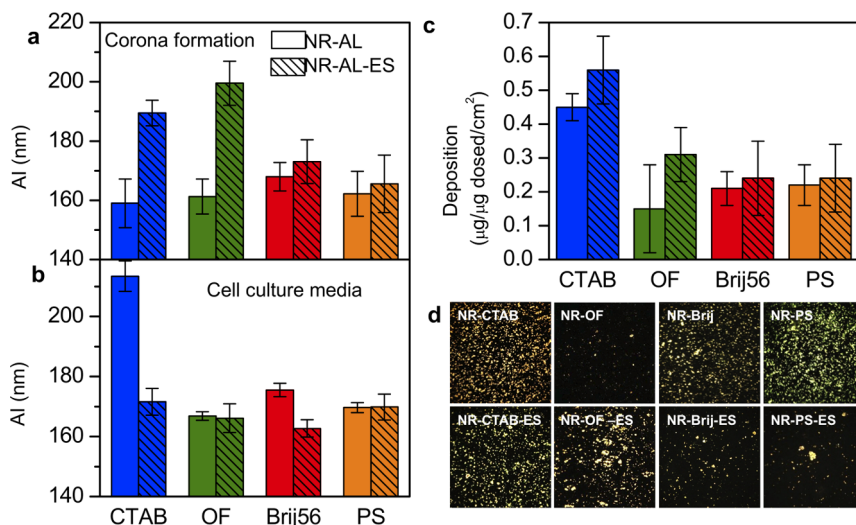


Figure 2. Colloidal stability based on aggregation index (AI) calculated from absorption spectra of NR-AL and NR-AL-ES in (a) water and (b) RPMI cell culture media. Error bars indicate standard deviation. (c) Analysis of the deposited gold content on the coverslips using ICP-MS for the various NR-AL and NR-AL-ES. (d) Darkfield (DF) imaging showing the deposition of NR-AL and NR-AL-ES onto glass coverslips coated with collagen after a 6 h exposure.

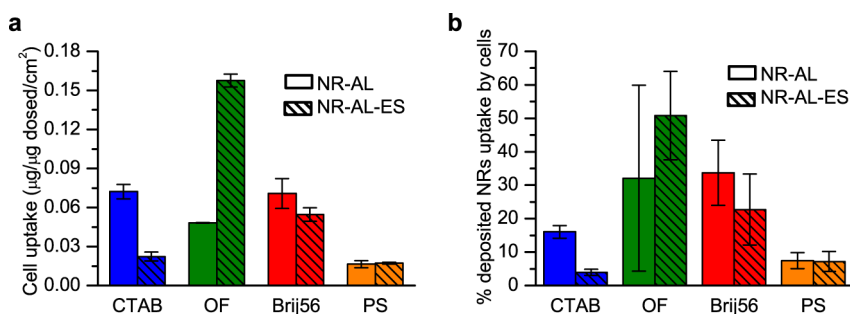


Figure 3. (a) Cell uptake normalized to the dosing following a 6 h exposure of NR-AL and NR-AL-ES in HaCaT cells as determined from ICP-MS. (b) Cell uptake of NR-AL and NR-AL-ES as a percentage of deposited NRs on the cell (Figure 2c). Error bars indicate standard deviation.

keratinocyte (HaCaT) cell line after a 6 h exposure in serum-free media. Uptake was quantified by measuring the amount of Au in the cells using ICP-MS normalized to the exposure concentration and visualized using DF microscopy (Figure 3a and Supporting Information, Figure S1) and TEM (Figure 4). In the absence of protein coronas, cell uptake was dependent on the ligands on NR-ALs, where both the positively charged and the neutral ALs generally had a higher uptake compared to negatively charged AL (PS). The high uptake of cationic NPs in serum-free environments has been reported in the literature and can be attributed to increased charge interaction between the cationic surface and the negatively charged cell membrane, which results in membrane disruption.¹⁹ The converse was true for NR-PS, which showed low uptake that was most likely due to unfavorable charge interaction with the negatively charged cell membrane. Despite being neutral, NR-Brij56 exhibited unexpectedly high uptake. This could be attributed to other favorable properties of the Brij56 headgroup, e.g., hydrophilicity, which promotes interaction with the cell membrane.

Because protein corona formation results in a negatively charged species (Figure 1b), this could account for the decrease in cell uptake for NR-CTAB-ES and NR-Brij56-ES. Furthermore, NR-CTAB-ES agglomerates were large ($D_H = 699.1$ nm) compared to NR-CTAB ($D_H = 8.6$ nm), which may have hindered the endocytosis mechanism in HaCaT cells. NR-OF-ES exhibited a significantly greater amount of uptake compared to all of the other samples ($p < 0.05$), apparently aided by the ability of OF to facilitate intracellular uptake. The mechanism may be due to a combination of favorable agglomerate size, stability compared to NR-OF, and an affinity of OF for cellular internalization. While this high uptake cannot be explained in terms of electrostatics, it agrees with results in the literature that OF has high delivery efficiency after interaction with serum proteins.³⁸ The exact composition of OF is proprietary, but it is most likely similar to another commercially available DNA transfection agent, Lipofectin, which is a mixture of a positively charged lipid, *N*-[1-(2,3-dioleyloyx)propyl]-*N,N,N*-trimethylammonium chloride (DOTMA), and a neutral colipid, dioleoylphosphatidylethanolamine (DOPE), required for stabilization

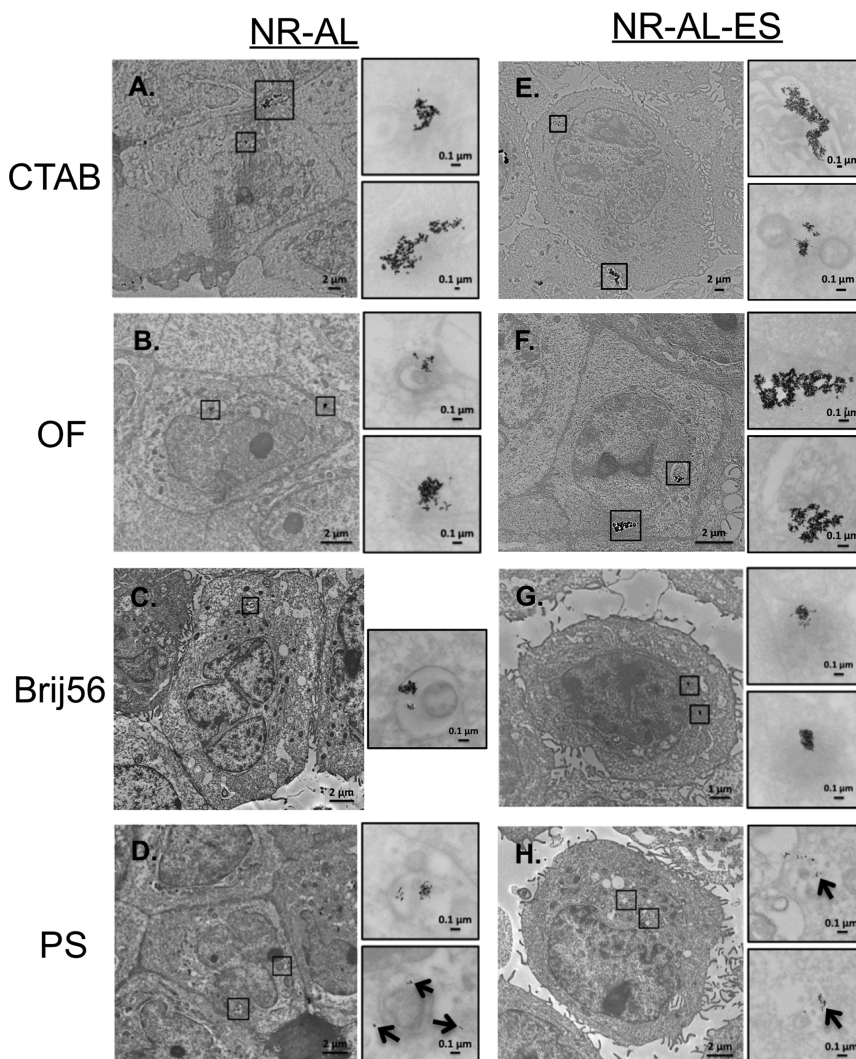


Figure 4. TEM images showing the uptake of NR-AL and NR-AL-ES into the HaCaT cells.

of the agent. A similar lipid mixture would yield a net positive charge for NR-OF. Together, they may interact with the serum proteins in a more complex manner yet maintain a reasonable $\Delta D_H = 174.1$ nm to give the unexpectedly high uptake.

The uptake for NR-Brij56-ES and NR-PS-ES did not differ significantly from the NRs with no corona proteins. This is expected given minimal corona formation of the NR-PS with the serum proteins. These results suggest that the cell uptake of NR-AL-ES is highly dependent on the nature of the AL, which dictates how it interacts with the serum proteins to yield different sized species and biological identities and hence different cell uptakes.

The TEM images provide qualitative information regarding the uptake and intracellular localization of the NRs. Large agglomerates appeared to be located in the extracellular space in both NR-AL and NR-AL-ES, such as for NR-CTAB and NR-CTAB-ES (Figure 4a, lower insert, and Figure 4e, upper insert). Uptake of smaller agglomerates, ~100–300 nm in size, was also observed. NR-OF agglomerates about ~100–200 nm in

size appeared to be taken up into small endosomes (Figure 4b). NR-OF-ES appeared to be taken up as much larger agglomerates (0.5–1 μ m, Figure 4f) and also showed higher uptake by ICP-MS. NR-Brij56 and NR-Brij56-ES were taken up into endosomes as agglomerates ~200 nm in size (Figure 4c). NR-PS and NR-PS-ES (Supporting Information, Figure S1d,h) seemed to assemble at the cell membrane, which others have attributed to electrostatic attraction to cationic sites on the membrane.³⁹ Very small agglomerates composed of 2–10 NRs were also observed, in addition to some slightly larger agglomerates approaching 100 nm (Figure 4d,h). Regardless of the small intracellular agglomerate sizes, the intracellular compartments still appeared large (close to 0.5 μ m), which would implicate a nonspecific endocytosis method.^{40,41} The corresponding DF images are available in the Supporting Information (Figure S1).

As the uptake of NRs was also dependent on their dosimetry, we investigated the deposition of NRs as a measure of dosimetry using ICP-MS and DF microscopy. We also calculated a predicted deposition fraction using

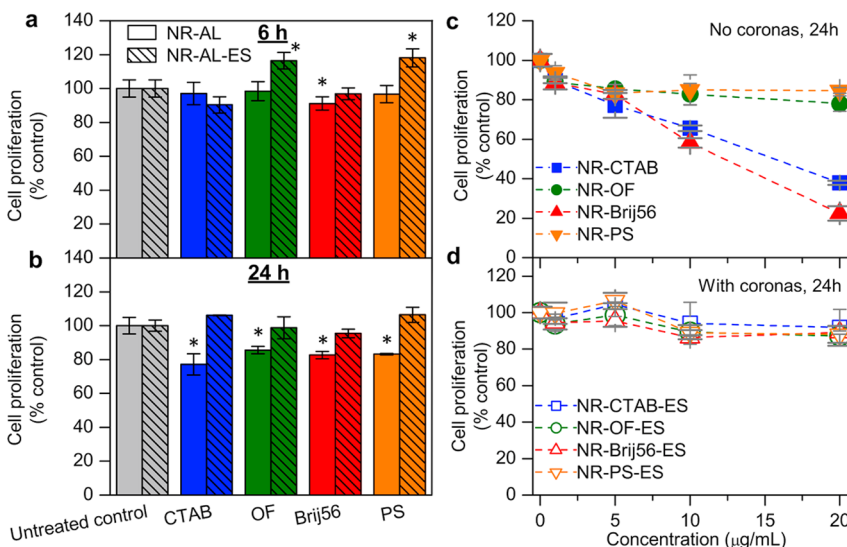


Figure 5. Cell proliferation of HaCaT cells using a live cell AlamarBlue assay after exposing the cells with 5 $\mu\text{g}/\text{mL}$ of NR-AL (solid bars) and NR-AL-ES (hatched bars) for 6 h and examining the response at the (a) 6 h time point and (b) 24 h time point. Exposure response curve for (c) NR-AL and (d) NR-AL-ES after exposing the cells to a range of concentrations from 1 to 20 $\mu\text{g}/\text{mL}$ for 6 h and examining the response at the 24 h time point. Error bars indicate standard deviation. The asterisks indicate statistical significance ($p < 0.05$) using a Student's *t* test. *P* values are given in the Supporting Information.

the *In Vitro* Sedimentation, Diffusion, and Dosimetry model, in which the dosimetry is ultimately a function of NR agglomerate diameter and effective density (Supporting Information, Table S2).⁴² Changing the AL and resulting corona demonstrated differences in agglomeration, so we expect that this can change the amounts of NRs that are deposited on the cells and available for cell uptake.^{42,43} If deposition and uptake exhibit similar trends, then uptake data is not a clear indication of affinity for the cells to take up the NRs, but of dosimetry.

The results show a statistically higher NR deposition for NR-CTAB and NR-CTAB-ES compared to other species (Figure 2c, blue, and Figure 2d). The sedimentation rate is directly proportional to the square of the particle diameter. Therefore, the high deposition for NR-CTAB may be due to the formation of larger agglomerates, indicated by the formation of a large protein corona (Figure 1c) and a high AI in cell culture media (Figure 2b). However, the data for hydrodynamic diameter did not follow the same trend, so we did not find good correlation between theoretical predictions and measured data for NR deposition (see the Supporting Information Table S2).

To decouple the effect of deposition (*i.e.*, dosimetry) on the cell uptake, we show the percentage of deposited NRs that were taken up into the cells (Figure 3b). Despite the high deposition of NR-CTAB and NR-CTAB-ES, their uptake was less than that of NR-Brij56, NR-OF, and their respective corona counterparts, confirming the low affinity for the cells to take up the NR-CTAB and NR-CTAB-ES instead of a low applied dose.

In the same manner, despite NR-PS and NR-PS-ES having similar deposition amounts as NR-Brij56 and

NR-Brij56-ES (Figure 2c,d), uptake was much lower for NR-PS and NR-PS-ES. This lower uptake is not because less NR-PS and NR-PS-ES reached the cell layer due to lower diffusive and sedimentation forces but that the chemical and biological nature of NR-PS has lower affinity with cells. The high variability in deposition for NR-OF is presumed to be related to low stability and uniformity, evidenced by visible sedimentation in the stock vial (Figure 2c). NR-OF-ES also showed comparable deposition to NR-Brij56-ES and NR-PS-ES; hence, its much higher cell uptake was not attributed to their higher dosimetry but rather to the high affinity of the cells to take up NR-OF-ES.

We note from our results that we can only conclude that the colloidal stability of NRs depends on AL type and presence of a corona, and that the AL type and presence of a corona influence the cell uptake ability. However, we cannot conclude with confidence if there is a link between the colloidal stability of the NRs and its cell uptake. Although our deposition study suggests a possible link, establishing a link between stability, protein corona and cell uptake would warrant a separate further study that examines this relationship systematically.

Influence of AL and Corona Formation on Cell Proliferation.

We also examined the proliferation of HaCaT cells using a live cell alamarBlue assay after exposing the cells with 5 $\mu\text{g}/\text{mL}$ of NRs for 6 h and examining the response at 6 and 24 h. At this exposure, the cytotoxicity of NR-ALs was low, where cell proliferation was not hindered and maintained at least 77.2% of control after 24 h (Figure 5a,b). There was an insignificant difference in cell proliferation between the four different NR-ALs.

At the 6 h time point, cells exposed to NR-AL-ES generally had increased proliferation relative to NR-AL for almost all ALs with the exception of NR-CTAB-ES, where the cell proliferation did not appear to be affected by corona formation ($90.3 \pm 4.9\%$ for NR-CTAB-ES vs $97.1 \pm 6.6\%$ for NR-CTAB, Figure 5a). The increase in cell proliferation was most pronounced for NR-PS-ES ($118.1 \pm 5.3\%$), followed by NR-OF-ES ($116.5 \pm 4.9\%$). The NR-Brij56-ES ($96.9 \pm 3.5\%$) was not significantly affected. The increase in proliferation in comparison to NR-AL without coronas also follows in the same order: +21.5% for NR-PS, +18.0% for NR-OF, and +5.7% for NR-Brij56.

Evidently, the presence and uptake of NR-AL-ES seem to encourage the HaCaT cells to multiply and proliferate, and the increase in proliferation seems to be ligand dependent. Because the serum proteins in the corona are essential for the growth and proliferation of cells, the protein corona may be enhancing the delivery of serum proteins into the cells to promote proliferation relative to cells that were not exposed to NR-AL-ES. For this same reason, because NR-CTAB-ES exhibited low cell uptake (Figure 3), it was not as effective in delivering the serum proteins in the corona into HaCaT cells. This probably explains the insignificant impact of corona formation on cell proliferation for NR-CTAB-ES.

The increase in proliferation due to corona formation was also observed at the 24 h time point for all NR-AL-ES compared to NR-AL, although the proliferation of NR-AL decreased between 6 and 24 h. To ensure that the decrease in proliferation observed for NR-AL with time is not due to the presence of endotoxin in the NR-AL samples, the NR stock solutions were tested for endotoxin using a Limulus Amebocyte Lysate endotoxin assay kit (Supporting Information, Figure S3). The endotoxin concentration was 0.033 ng/mL in the media and ranged from 0.076 to 0.089 ng/mL in the NR samples. These values were considered insignificant based on a previous study, which showed that up to 20 ng/mL of lipopolysaccharide did not affect the proliferation of 7 cell-lines.⁴⁴

We increased the exposure for both NR-AL and NR-AL-ES to examine the exposure response on HaCaT cell proliferation after 24 h. In the absence of coronas, both NR-OF and NR-PS did not exhibit an observable dose dependence on the cell proliferation up to the highest exposure of $20 \mu\text{g/mL}$ (Figure 5c). On the other hand, NR-CTAB and NR-Brij56 resulted in a decrease in cell proliferation from 89.8% to 22.4% as their concentration was increased from 1 to $20 \mu\text{g/mL}$, with 50% Growth Inhibition, GI₅₀, $15 \mu\text{g/mL}$ for both ALs. With the formation of a protein corona, cell proliferation of all four NR-AL-ES showed markedly less dependence on the exposure (Figure 5d). This was particularly true for NR-CTAB-ES and NR-Brij56-ES, where their cell proliferation maintained at least 86.5% at the highest exposure of $20 \mu\text{g/mL}$. This observation that the

protein corona plays an important role in minimizing the cytotoxicity has also been observed and reported in other studies.^{14,45}

Influence of Pen/Strep on Cell Response for NR-ALs with and without Coronas. NR-AL-ES have been found to have high capacity for small molecule payloads.³² In cell response studies, antibiotic supplements are necessary for cell culture, and these can potentially interact with the NR-AL-ES. We found that the presence of penicillin/streptomycin (pen/strep), a commonly used antibiotic supplement for preventing bacteria growth in cell culture media, also affected the colloidal stability of NR-ALs (Figure 6a). The AI of all four NR-ALs in cell culture media increased in the presence of pen/strep, indicating that NR-ALs interact with pen/strep in a way that decreases their colloidal stability. Unlike corona formation, cell uptake of NR-CTAB and NR-Brij56 remained unaffected by the presence of pen/strep, while uptake of NR-OF and NR-PS was increased (Figure 6b). Because they are composed of phospholipids, OF and PS could have a greater degree of interaction with pen/strep and the cell membrane compared to CTAB and Brij56 to result in increased uptake over the absence of pen/strep.

This same interaction could have also caused the significant reduction in cell proliferation by NR-OF and NR-PS in the presence of pen/strep (Figure 6c). Even though pen/strep is not toxic to eukaryotic cells at normal cell culture concentrations, the interaction with the cell membrane and higher cell uptake could increase the permeability of the cells to antibiotics. Increased cell permeability during cell uptake may cause high antibiotic influx beyond the tolerable intracellular concentration of pen/strep, leading to antibiotic toxicity. Higher cell death is known to occur when antibiotics are present during transfection in common transfection protocols.⁴⁶ This could also explain why the cells showed higher levels of oxidative stress with NR-ALs in the presence of pen/strep (Figure 6d).

With the protein corona, the presence of pen/strep in the cell culture media also increased the AI of all four NR-AL-ES, although the extent of aggregation induced by pen/strep was lower compared to NR-AL as evidenced by smaller changes in their AI (Figure 7a). This increase in AI with protein corona in the presence of pen/strep was also observed by Hühn *et al.*³⁴ and shows that the corona makes the NRs less susceptible to pen/strep-induced aggregation. The presence of pen/strep also seemed to promote cell uptake of all four NR-AL-ES, with the most prominent increase in cell uptake for NR-OF-ES (Figure 7b), as was also observed with NR-OF. In this case, NR-OF-ES exhibited the highest cell uptake of $0.22 \mu\text{g}/\mu\text{g}$ exposed/cm² among all the experiments. The presence of pen/strep during cell uptake of NR-AL-ES has also led to reduced cell proliferation (Figure 7c) and higher levels of oxidative stress (Figure 7d) for all NR-AL-ES, as discussed

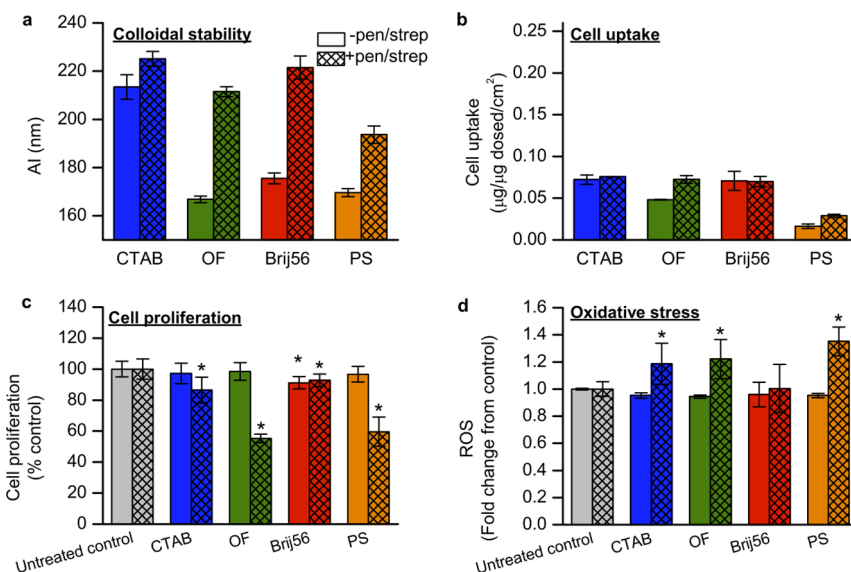


Figure 6. Comparison of the effect of 100 units/mL of penicillin/streptomycin (Pen/Strep) in cell culture media on NR-AL in terms of the (a) colloidal stability as determined by AI; (b) cell uptake as determined by ICP-MS; (c) cell proliferation as determined by AlamarBlue assay; and (d) oxidative stress as determined by the change in generation of ROS. The exposure conditions are the same as previous studies. Error bars indicate standard deviation. The asterisks indicate statistical significance ($p < 0.05$) using a Student's *t* test. *P* values are given in the Supporting Information.

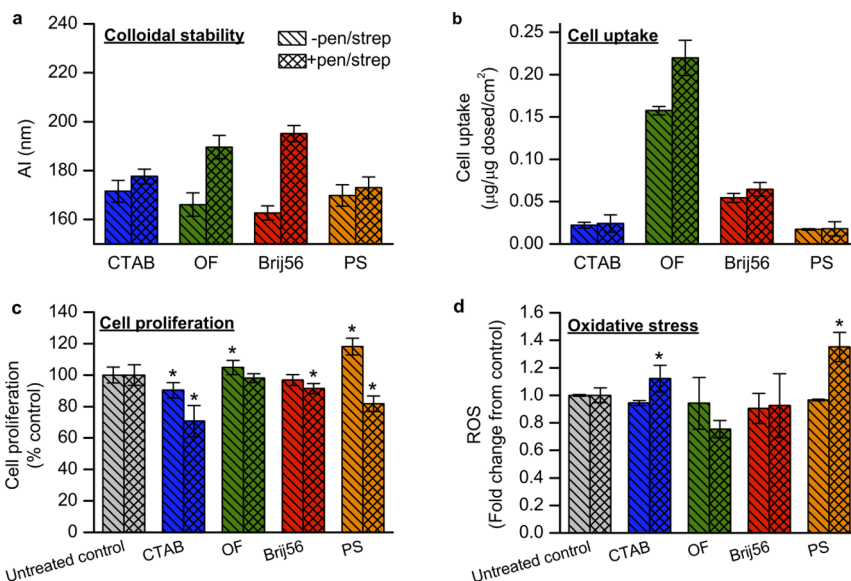


Figure 7. Comparison of the effect of 100 units/mL of penicillin/streptomycin (Pen/Strep) in cell culture media on NR-AL-ES in terms of the (a) colloidal stability as determined by AI, (b) cell uptake as determined by ICP-MS, (c) cell proliferation as determined by AlamarBlue assay, and (d) oxidative stress as determined by the change in generation of ROS. The exposure conditions are the same as previous studies. Error bars indicate standard deviation. The asterisks indicate statistical significance ($p < 0.05$) using a Student's *t* test. *P* values are given in the Supporting Information.

previously. This is empirical evidence that, apart from serum proteins in cell culture which led to formation of protein corona, other often overlooked cell culture supplements such as pen/strep may play an important role in altering the physical properties of NR-ALs such as colloidal stability, thereby affecting the cellular response.

Influence of NR-AL-ES and Pen/Strep on Gene Expression Related to Oxidative Stress and Inflammation. We examined the influence of NR-AL-ES and pen/strep on gene expression to understand which molecular mechanisms

in the cells were impacted. In general, there were more common genes regulated than unique genes and there was no trend in gene expression related to the charge of the NR-ALs.

However, there did appear to be a trend in gene expression related to the presence or absence of pen/strep. NR-AL-ES with pen/strep resulted in an up-regulation of genes associated with oxidative stress (Table 1). *FMO5* and *EPHX2* were significantly up-regulated by all four NR-AL-ES. The up-regulation of

TABLE 1. Genes Significantly Affected by Exposure to NR-AL-ES and Its Relation to the Presence of Pen/Strep: Oxidative Stress and Inflammation^a

pen/strep	NR-CTAB-ES		NR-OF-ES		NR-Brij56-ES		NR-PS-ES		Function
	-	+	-	+	-	+	-	+	
FMO5	NA	4.9 (0.002)	NA	10.4 (0.0008)	NA	5.9 (0.0002)	NA	6.9 (0.001)	oxidative stress
EPHX2	NA	8.6 (0.011)	NA	14.2 (0.002)	NA	11.5 (0.0001)	NA	6.6 (0.014)	oxidative stress
IL1B	4.4 (0.0005)	-15.4 (0.0004)	5.8 (0.005)	-4.7 (0.007)	22.4 (0.001)	-13.0 (0.0005)	32.5 (0.0001)	-5.0 (0.008)	inflammation
IL6	3.2 (0.004)	-8.4 (0.0006)	4.2 (0.004)	-4.8 (0.003)	21.2 (0.0005)	-47.6 (0.0001)	15.0 (0.0002)	-7.3 (0.005)	inflammation
PAI-1	1.2 (0.511)	-1.3 (0.403)	-1.3 (0.639)	-2.4 (0.029)	6.9 (0.004)	-4.9 (0.0006)	2.1 (0.034)	-2.9 (0.005)	inflammation
TNF	7.0 (0.006)	-3.5 (0.0038)	3.9 (0.048)	2.9 (0.022)	41.0 (0.0005)	-2.2 (0.023)	27.0 (0.003)	1.9 (0.042)	inflammation

^a Numbers indicate fold regulation; NA indicates no significant change, (student's t test, $p < 0.05$). Significant up-regulation >1.5 in green, down-regulation <1.5 in red.

TABLE 2. Genes Significantly Affected by Exposure to NR-AL-ES and Its Relation to the Presence of Pen/Strep: DNA Damage and Cell Cycle^a

pen/strep	NR-CTAB-ES		NR-OF-ES		NR-Brij56-ES		NR-PS-ES		Function
	-	+	-	+	-	+	-	+	
ATM	-1.3 (0.540)	2.3 (0.032)	-1.4 (0.388)	3.1 (0.082)	1.7 (0.424)	2.9 (0.014)	1.2 (0.677)	4.0 (0.003)	DNA damage and repair
TP53	-1.2 (0.006)	1.7 (0.256)	-1.3 (0.011)	2.8 (0.017)	1.1 (0.858)	1.7 (0.041)	-1.5 (0.010)	2.3 (0.021)	DNA damage and repair
CDKN1A	1.2 (0.487)	1.6 (0.220)	1.2 (0.457)	1.6 (0.285)	6.9 (0.015)	1.7 (0.043)	3.0 (0.010)	1.2 (0.530)	cell cycle checkpoint/arrest
GADD45A	1.7 (0.126)	-4.5 (0.0004)	2.5 (0.071)	-2.6 (0.012)	5.0 (0.012)	-5.5 (0.0003)	3.8 (0.011)	-3.4 (0.006)	growth arrest and senescence

^a Numbers indicate fold regulation (student's t test, $p < 0.05$). Significant up-regulation >1.5 in green, down-regulation <1.5 in red.

oxidative stress genes correlates with increased ROS production in cells (Figure 7d). This suggests that toxicity observed for NR-AL-ES in the presence of pen/strep may be partially mediated by oxidative stress.

In the presence of pen/strep, genes associated with inflammation, including *IL6* and *IL1B*, were down-regulated for NR-AL-ES (Table 1). The down-regulation of genes associated with a pro-inflammatory response after exposure to NRs was previously attributed to the anti-inflammatory property of gold.^{18,47} However, *IL6* and *IL1B* were up-regulated for NR-AL-ES without the presence of pen/strep. Since the previous studies were conducted in the presence of pen/strep, there may be a unique phenomenon occurring related to the adsorption and intracellular delivery of pen/strep in the presence of Au nanoparticles.

Additional genes associated with inflammation, including *PAI-1* and *TNF*, were regulated by NR-AL-ES. *PAI-1* encodes a protein that plays a role in cell movement, inflammation, and proliferation.⁴⁸ *PAI-1* was significantly down-regulated by NR-OF-ES, NR-Brij56-ES,

and NR-PS-ES with the presence of pen/strep and up-regulated by the NR-Brij56-ES and NR-PS-ES without the presence of pen/strep (Table 1). The tumor necrosis factor (TNF) superfamily is complex, and the ligands and their receptors can activate cell apoptosis, proliferation, differentiation, or survival.⁴⁹ *TNF* is a pro-inflammatory cytokine belonging to the TNF superfamily and is involved in the regulation of many of these processes. *TNF* was down-regulated for NR-CTAB-ES and NR-Brij56-ES and up-regulated for NR-OF-ES and NR-PS-ES in the presence of pen/strep. Up-regulation was observed when pen/strep was not present (Table 1). We tested the endotoxin concentration in the stock NR solutions to ensure that the up-regulation of inflammatory genes without pen/strep was not due to contamination (Supporting Information, Figure S3).

Influence of NR-AL-ES and Pen/Strep on Gene Expression Related to DNA Damage and Cell Cycle. Genes related to DNA damage and the cell cycle were also regulated (Table 2). *ATM* was up-regulated after exposure to NR-AL-ES in the presence of pen/strep, which is activated

in response to DNA damage. A target of ATM activation includes *TP53*, which was also up-regulated by NR-AL-ES in the presence of pen/strep. CDK inhibitors (CDKN) prevent the cell cycle from progressing during DNA repair.⁵⁰ *CDKN1A* was up-regulated by NR-Brij56-ES both with and without the presence of pen/strep and NR-PS-ES without the presence of pen/strep.

GADD45A is another target that regulates DNA repair, plays a role in growth arrest, senescence, and apoptosis, and was down-regulated by all NR-AL-ES in the presence of pen/strep. Down-regulation of *GADD45A* was also observed for NR-PEG (poly(ethylene glycol)) and NR-MHDA (mercaptohexadecanoic acid) in a previous study.¹⁸ Up-regulation of *GADD45A* was observed for NR-AL-ES without pen/strep. Unique regulation of genes involved in DNA damage and repair for NR-AL-ES in the presence versus absence of pen/strep indicates toxicity associated with the presence of the antibiotic and may be related to the NRs being able to efficiently transfer pen/strep into the cell.

Together, these changes in gene expression are the results of both NR-AL-ES and pen/strep working in tandem to alter the molecular mechanisms in cells. They could lead to the overall reduction in cell proliferation (Figure 7c). These changes in gene expression show that the presence of pen/strep plays an important role in impacting the cell response of NR-ALs. Antibiotics are known to cause toxicity to some sensitive cell-lines during transfection.⁴⁶

SUMMARY AND CONCLUSIONS

It is evident that the corona properties are influenced by the underlying ligand on the surface of the NRs, and the cellular response varies as a consequence. Hence, the ALs play not a direct role but instead an intermediary one in affecting the cellular response of NR-ALs. The nature of the ALs affects the formation and physical characteristics of their preformed protein coronas, specifically the extent of corona formation (as evidenced by size), colloidal stability of the resulting species, and probably the corona composition. This is most likely due to the fact that the AL ligand can come on and off the NR surface to interact

with the different corona proteins more intimately than a covalently attached ligand.

Corona formation not only stabilizes the NR-AL in cell culture media but also increases the overall hydrodynamic size of NR-AL-ES, possibly leading to reduced cell uptake as in the case of NR-CTAB-ES relative to NR-CTAB with no corona. While others have observed increased cellular uptake of NPs in upright cell culture due to sedimentation, where uptake is independent of size, shape, density, surface coating and initial concentration of the NPs,⁴³ we note that this may not be true for NPs with preformed protein coronas because they are more stable in cell culture media and hence have a lower tendency to aggregate and sediment. In other instances, corona formation can elicit stronger responses than for the NR-AL alone, such as for NR-OF on uptake, cell proliferation, and generation of ROS.

We also found that the presence of the cell culture supplement pen/strep can exert a significant impact on the colloidal stability and consequently the cellular response of NR-AL and NR-AL-ES. Specifically, NR-AL and NR-AL-ES in the presence of pen/strep also produces an unexpected difference in cell viability, proliferation, and oxidative stress, most likely due to the way it interacts with the corona proteins. Pen/strep has been shown to decrease particle stability,³⁴ and here we show that its impact on the cellular response is multifaceted. These results show that commonly used supplements such as antibiotics that are necessary for cell culture can also interact with the NR-AL and NR-AL-ES and potentially lead to unexpected side effects.

The results of this study suggest that in addition to a direct response to the surface ligands, the cellular behavior toward NR-AL is mediated not just by the protein corona it recruits, but also its resulting colloidal stability and interaction with cell culture supplements. Although the protein corona is what the cells see, the underlying surface ligands evidently play an important role in shaping and defining the physical characteristics of the corona, which ultimately impacts the cellular response. Therefore, rational design of the surface ligands can help us to define and perhaps exploit the corona for biological applications.

MATERIALS AND METHODS

Synthesis of NR-CTAB. NRs were first synthesized with their native amphiphilic surface ligand CTAB. Unless otherwise stated, all reagents used in the synthesis were obtained from Sigma-Aldrich and used as received. Milli-Q water with a resistivity of 18.2 MΩ cm was used for all experiments. CTAB coated gold NRs were synthesized using a nonseed-mediated approach.⁵¹ NR size was determined using transmission electron microscopy (TEM). NRs were washed once by centrifuging at 13000 rcf for 30 min and resuspended in water to remove excess reactants. NR concentration after washing was determined by optical absorption (Cary 100 UV-vis spectrophotometer, Agilent Technologies) and was typically ~1.5 nM. Washed NR-CTAB were kept at room temperature (20 °C) before further experiments.

Ligand Exchange and Characterization of NR-AL. CTAB was first replaced by Brij56 (Sigma-Aldrich) by centrifuging 1 mL of NR-CTAB at 13000 rcf for 20 min before removing the supernatant and adding 500 μL of 0.1 mM CTAB to the pellet. The solution was thoroughly mixed and centrifuged again at 9000 rcf for 20 min. The supernatant was removed, and 0.1 mM Brij56 was added to the pellet before incubation for 1 h at 37 °C. Excess Brij56 was then removed by centrifuging NR and washing them once in water for 15 min at 2000 rcf using centrifugal filters (Amicon Ultra, Millipore Ireland, Ltd.). The final volume recovered (40 μL) was diluted in water to give NR-Brij56. To prepare NR-OF, 50 μL of OF reagent (Invitrogen, Inc.) was added to 40 μL of NR-Brij56. The solution was mixed and aged overnight at 37 °C. Excess OF was removed, and the NR-OF was washed the same way as described previously for Brij56. To prepare the

NR-PS, 100 μ L of 20 mM PS (Avanti Polar Lipids, Inc.) was added to 40 μ L of NR-Brij56, mixed thoroughly, and aged overnight at 37 °C. The PS was purchased in powder form and dissolved in water to make a 20 mM solution. The NR-PS was washed to remove excess PS as previously described for Brij56 and OF. All the NR-ALs were stored at room temperature until used. Successful ligand exchange was probed by the zeta-potential of NR-ALs (Malvern Zetasizer Nano ZS90) and agarose gel electrophoresis in a 0.2% agarose gel in 0.5 X Tris-borate-EDTA (TBE) buffer. Gel electrophoresis was performed at 82 V for 60 min. The NR-ALs were also imaged using TEM to show that ligand exchange did not affect the primary size and morphology. The D_h was assessed using dynamic light scattering (Malvern Zetasizer Nano ZS90). The final concentration of the NRs was measured using inductively coupled plasma–mass spectrometry (ICP-MS) (Perkin Elmer NexION 300D).

Endotoxin Assay. The ToxinSensor Chromogenic LAL Endotoxin Assay Kit (GenScript) was used to test for endotoxin in the NR stock solutions. Each NR sample was diluted to 5 μ g/mL in LAL reagent water. A standard curve was prepared using dilutions of endotoxin standard solution. The assay was completed according to manufacturer's instructions. The absorbance was measured at 545 nm.

Formation of Protein Corona and Influence of Pen/Strep on Colloidal Stability. Prior to forming the protein corona, the NR-ALs were centrifuged at 2000 rcf for 20 min to obtain the pellet. Protein coronas were formed on NR-ALs by adding 500 μ L of 0.4% horse (equine) serum (ES) (ATCC, Inc.) in 5 mM phosphate buffer (PhB, pH 7.4) directly to the NR-AL pellet and incubating it at 37 °C for the corona to harden. Following an overnight incubation, the NR-AL-ES were then washed once with buffer to remove excess proteins, before reconstituting them in water or RPMI cell culture media in the absence and presence of pen/strep before further studies.

The colloidal stability of NR-AL and NR-AL-ES in water and RPMI cell culture media in the absence and presence of pen/strep was probed and quantified as an aggregation index (AI) by absorption spectroscopy (Cary 100 UV–vis spectrophotometer, Agilent Technologies) as described previously.³⁵ Since the longitudinal plasmon peak is highly sensitive to aggregation, the AI is a measure of the longitudinal surface plasmon resonance (LSPR) peak broadening derived from the total area under the absorption spectrum of the LSPR from 600 to 900 nm, divided by LSPR intensity. The AI gives the equivalent bandwidth of the longitudinal peak (with units of nm) for a spectrum normalized to the LSPR peak intensity. A higher degree of aggregation corresponds to a higher AI value.

Nanorod Deposition. Glass coverslips (5 mm, #1) were coated with collagen and then exposed to NR exposure dispersions for 6 h. The coverslips were transferred to a glass slide for imaging or to a conical tube for digestion and analysis of gold content. Imaging was performed using a darkfield (DF) condenser from CytoViva attached to an Olympus BX41 microscope and DAGE camera/software. A minimum of 3 coverslips per NR sample was rinsed extensively with aqua regia (3% HCl, 1% HNO₃). An internal standard was added (20 μ g/L), and then samples were analyzed using ICP-MS.

Cellular Uptake. Human keratinocyte (HaCaT) cells were seeded at 1 \times 10⁵ cells per cm² and maintained in RPMI culture media supplemented with 10% fetal bovine serum (FBS) and 1% pen/strep at 37 °C in a humidified 5% CO₂ and 95% air atmosphere. After 24 h, the cells were exposed to 5 μ g/mL (0.05 nM) of NR-AL and NR-AL-ES for 6 h in serum-deprived and pen/strep-deprived RPMI media, following which the NRs were removed and cells were washed thrice with 1 \times phosphate buffered saline (PBS). The cells were lysed, and the amount of Au in the cells was quantified using ICP-MS (PerkinElmer, NexION 300D). Cell uptake was quantified by measuring the amount of Au in the cells normalized to the exposure mass concentration.

The interaction of NRs with cells was evaluated using DF imaging and TEM. For DF imaging, cells were plated at a concentration of 1.0 \times 10⁵ cells/cm² in 2-chambered slides (surface area = 4 cm²) and allowed to proliferate and adhere for 24 h or until ~80% confluent. Cells were exposed to NRs at a concentration of 5 μ g/mL in media and exposed for 6 h. Following exposure, cells were washed with PBS and fixed in 4%

paraformaldehyde for 10 min. The cells were washed again with PBS, a coverslip was added and sealed with clear nail polish, and the slide was imaged using the CytoViva Hyperspectral Imaging System attached to an Olympus BX41 microscope (Aetos Technologies, Inc., Auburn, AL). Images were collected using DAGE camera/software.

For TEM imaging, cells were seeded at a concentration of 1.0 \times 10⁵ cells/cm² in 6-well plates (surface area = 9.6 cm²) and allowed to adhere and proliferate for 24 h. Cells were exposed to NRs diluted at a concentration of 5 μ g/mL in media and exposed for 6 h. Following exposure, cells were washed with PBS, trypsinized from the plate, and centrifuged at 1000 rcf for 10 min. The pellet was fixed in 2% paraformaldehyde and 2.5% glutaraldehyde overnight at 4 °C. The following day, the cell pellets were washed extensively with PBS, stained with 1% osmium tetroxide, and dehydrated with ethanol in a standard dilution sequence. The final pellet was embedded in LR White resin (EMS) and cured in a vacuum oven at 60 °C. The cured sample was sectioned using a Leica EM UC6 Ultramicrotome and imaged using a Hitachi H-7600 TEM at the Nanoscale Engineering Science and Technology Laboratory, University of Dayton.

Cell Proliferation and Oxidative Stress. The proliferation and oxidative stress in HaCaT cells were examined by preparing and exposing the cells in the same manner. The proliferation of HaCaT cells was examined as a function of NR concentration using a live cell alamarBlue assay according to the manufacturer's instructions (Invitrogen). The oxidative stress was examined using a fluorescent probe to detect reactive oxygen species (ROS). Briefly, a 10 mM working stock of 2',7'-dichlorofluorescein-diacetate (DCFH–DA) (Invitrogen) was dissolved in DMSO. The stock was further diluted in RPMI culture media to 100 μ M. The 100 μ M DCFH–DA solution was preincubated with the cells for 20 min at 37 °C, after which it was removed, and the exposure solutions were added. A standard curve was prepared using H₂O₂ (100 μ M to 3 mM). The plate was read at Ex 485/Em 530 nm. The same experiments were repeated with NR-AL and NR-AL-ES in RPMI in the presence of 100 units/mL of pen/strep.

Gene Expression. Real-time reverse transcriptase polymerase chain reaction (RT-PCR) was used to evaluate gene expression by HaCaT cells when exposed to NRs at 5 μ g/mL. Cells were seeded and exposed to NR-AL-ES as described above (1 \times 10⁵ cells/cm²) in serum-deprived and pen/strep-deprived RPMI media. After a 6 h exposure, RNA was isolated from the cells using a RNA Isolation Kit (Qiagen). The RNA yield was determined using a NanoDrop spectrophotometer (ThermoScientific). Following RNA isolation, c-DNA was prepared using the RT2 First Strand kit (SABiosciences) according to the manufacturer's instructions. The stress and toxicity array (SABiosciences) was used to evaluate the expression of genes involved in pathways activated by stress.

Data was analyzed based on average threshold cycles (Ct), which is equal to the cycle number at which fluorescence generated crosses the fluorescence threshold. The Ct values were normalized based on the mean of Ct values for a set of five housekeeping genes for each trial. Fold regulation was determined for each test sample versus the negative control based on an inverse relationship of the normalized Ct values, which were averaged for triplicate trials. Genes that were significantly different for NR-AL-ES versus the negative control were determined by a Student's *t* test comparing the normalized Ct values for each test sample to the negative control. The same experiments were repeated with NR-AL-ES in RPMI in the presence of 100 units/mL pen/strep.

Conflict of Interest: The authors declare no competing financial interest.

Acknowledgment. Funding was from the NSF (DMR No. 0906838). J.C.Y.K was supported by the NUS OPF. We thank Z. Xu for TEM imaging and the MIT Center for Materials Science and Engineering for use of the TEM. We thank the Bawendi group for use of their zetasizer. C.G. was supported by an ORISE fellowship.

Supporting Information Available: DF microscopy images of cell uptake, endotoxin assay, ROS assays, *p* values of relevant data, and theoretical dosimetry results. This material is available free of charge via the Internet at <http://pubs.acs.org>.

REFERENCES AND NOTES

- Lundqvist, M.; Stigler, J.; Elia, G.; Lynch, I.; Cedervall, T.; Dawson, K. A. Nanoparticle Size and Surface Properties Determine the Protein Corona with Possible Implications for Biological Impacts. *Proc. Natl. Acad. Sci. U.S.A.* **2008**, *105*, 14265–14270.
- Podila, R.; Chen, R.; Ke, P. C.; Brown, J. M.; Rao, A. M. Effects of Surface Functional Groups on the Formation of Nanoparticle-Protein Corona. *Appl. Phys. Lett.* **2012**, *101*, 263701.
- Walkey, C. D.; Olsen, J. B.; Guo, H. B.; Emili, A.; Chan, W. C. W. Nanoparticle Size and Surface Chemistry Determine Serum Protein Adsorption and Macrophage Uptake. *J. Am. Chem. Soc.* **2012**, *134*, 2139–2147.
- Jedlovszky-Hajdú, A.; Bombelli, F. B.; Monopoli, M. P.; Tombacz, E.; Dawson, K. A. Surface Coatings Shape the Protein Corona of SPIONS with Relevance to Their Application *In Vivo*. *Langmuir* **2012**, *28*, 14983–14991.
- Cukalevski, R.; Lundqvist, M.; Oslakovic, C.; Dahlback, B.; Linse, S.; Cedervall, T. Structural Changes in Apolipoproteins Bound to Nanoparticles. *Langmuir* **2011**, *27*, 14360–14369.
- Pan, H.; Qin, M.; Meng, W.; Cao, Y.; Wang, W. How Do Proteins Unfold Upon Adsorption on Nanoparticle Surfaces? *Langmuir* **2012**, *28*, 12779–12787.
- Tellechea, E.; Wilson, K. J.; Bravo, E.; Hamad-Schifferli, K. Engineering the Interface between Glucose Oxidase and Nanoparticles. *Langmuir* **2012**, *28*, 5190–5200.
- Salvati, A.; Pitek, A. S.; Monopoli, M. P.; Prapainop, K.; Bombelli, F. B.; Hristov, D. R.; Kelly, P. M.; Åberg, C.; Mahon, E.; Dawson, K. A. Transferrin-Functionalized Nanoparticles Lose Their Targeting Capabilities When a Biomolecule Corona Adsorbs on the Surface. *Nat. Nanotechnol.* **2013**, *8*, 137–143.
- Mirshafiee, V.; Mahmoudi, M.; Lou, K.; Cheng, J.; Kraft, M. L. Protein Corona Significantly Reduces Active Targeting Yield. *Chem. Commun.* **2013**, *49*, 2557–2559.
- Dell'Orco, D.; Lundqvist, M.; Cedervall, T.; Linse, S. Delivery Success Rate of Engineered Nanoparticles in the Presence of the Protein Corona: A Systems-Level Screening. *Nanomed Nanotechnol Biol. Med.* **2012**, *8*, 1271–1281.
- Hirn, S.; Semmler-Behnke, M.; Schleeh, C.; Wenk, A.; Lipka, J.; Schäffler, M.; Takenaka, S.; Möller, W.; Schmid, G.; Simon, U.; et al. Particle Size-Dependent and Surface Charge-Dependent Biodistribution of Gold Nanoparticles after Intravenous Administration. *Eur. J. Pharm. Biopharm* **2011**, *77*, 407–416.
- Deguchi, S.; Yamazaki, T.; Mukai, S.; Usami, R.; Horikoshi, K. Stabilization of C₆₀ Nanoparticles by Protein Adsorption and Its Implications for Toxicity Studies. *Chem. Res. Toxicol.* **2007**, *20*, 854–858.
- Drescher, D.; Orts-Gil, G.; Laube, G.; Natte, K.; Veh, R. W.; Österle, W.; Kneipp, J. Toxicity of Amorphous Silica Nanoparticles on Eukaryotic Cell Model Is Determined by Particle Agglomeration and Serum Protein Adsorption Effects. *Anal. Bioanal. Chem.* **2011**, *400*, 1367–1373.
- Ge, C. C.; Du, J. F.; Zhao, L. N.; Wang, L. M.; Liu, Y.; Li, D. H.; Yang, Y. L.; Zhou, R. H.; Zhao, Y. L.; Chai, Z. F.; et al. Binding of Blood Proteins to Carbon Nanotubes Reduces Cytotoxicity. *Proc. Natl. Acad. Sci. U.S.A.* **2011**, *108*, 16968–16973.
- Babaj, A.; Samanta, B.; Yan, H.; Jerry, D. J.; Rotello, V. M. Stability, Toxicity and Differential Cellular Uptake of Protein Passivated-Fe₃O₄ Nanoparticles. *J. Mater. Chem.* **2009**, *19*, 6328–6331.
- Maiorano, G.; Sabella, S.; Sorce, B.; Brunetti, V.; Malvindi, M. A.; Cingolani, R.; Pompa, P. P. Effects of Cell Culture Media on the Dynamic Formation of Protein–Nanoparticle Complexes and Influence on the Cellular Response. *ACS Nano* **2010**, *4*, 7481–7491.
- Wang, G. K.; Papasani, M. R.; Cheguru, P.; Hrdlicka, P. J.; Hill, R. A. Gold–Peptide Nanoconjugate Cellular Uptake Is Modulated by Serum Proteins. *Nanomed Nanotechnol Biol. Med.* **2012**, *8*, 822–832.
- Grabinski, C.; Schaeublin, N.; Wijaya, A.; D'Couto, H.; Baxamusa, S. H.; Hamad-Schifferli, K.; Hussain, S. M. Effect of Gold Nanorod Surface Chemistry on Cellular Response. *ACS Nano* **2011**, *5*, 2870–2879.
- Oh, W. K.; Kim, S.; Choi, M.; Kim, C.; Jeong, Y. S.; Cho, B. R.; Hahn, J. S.; Jang, J. Cellular Uptake, Cytotoxicity, and Innate Immune Response of Silica-Titania Hollow Nanoparticles Based on Size and Surface Functionality. *ACS Nano* **2010**, *4*, 5301–5313.
- Mortensen, N. P.; Hurst, G. B.; Wang, W.; Foster, C. M.; Nallathambi, P. D.; Retterer, S. T. Dynamic Development of the Protein Corona on Silica Nanoparticles: Composition and Role in Toxicity. *Nanoscale* **2013**, *5*, 6372–6380.
- Alkilany, A. M.; Shatanawi, A.; Kurtz, T.; Caldwell, R. B.; Caldwell, R. W. Toxicity and Cellular Uptake of Gold Nanorods in Vascular Endothelium and Smooth Muscles of Isolated Rat Blood Vessel: Importance of Surface Modification. *Small* **2012**, *8*, 1270–1278.
- Lee, S. E.; Sasaki, D. Y.; Park, Y.; Xu, R.; Brennan, J. S.; Bissell, M. J.; Lee, L. P. Photonic Gene Circuits by Optically Addressable Sirna-Au Nanoantennas. *ACS Nano* **2012**, *6*, 7770–7780.
- Lee, S. E.; Sasaki, D. Y.; Perroud, T. D.; Yoo, D.; Patel, K. D.; Lee, L. P. Biologically Functional Cationic Phospholipid-Gold Nanoplasmonic Carriers of RNA. *J. Am. Chem. Soc.* **2009**, *131*, 14066–14074.
- Li, P. C.; Li, D.; Zhang, L. X.; Li, G. P.; Wang, E. K. Cationic Lipid Bilayer Coated Gold Nanoparticles-Mediated Transfection of Mammalian Cells. *Biomaterials* **2008**, *29*, 3617–3624.
- Orendorff, C. J.; Alam, T. M.; Sasaki, D. Y.; Bunker, B. C.; Voigt, J. A. Phospholipid-Gold Nanorod Composites. *ACS Nano* **2009**, *3*, 971–983.
- Takahashi, H.; Niidome, Y.; Niidome, T.; Kaneko, K.; Kawasaki, H.; Yamada, S. Modification of Gold Nanorods Using Phosphatidylcholine to Reduce Cytotoxicity. *Langmuir* **2006**, *22*, 2–5.
- Ba, H. J.; Rodríguez-Fernández, J.; Stefani, F. D.; Feldmann, J. Immobilization of Gold Nanoparticles on Living Cell Membranes Upon Controlled Lipid Binding. *Nano Lett.* **2010**, *10*, 3006–3012.
- Alkilany, A. M.; Nagaria, P. K.; Hexel, C. R.; Shaw, T. J.; Murphy, C. J.; Wyatt, M. D. Cellular Uptake and Cytotoxicity of Gold Nanorods: Molecular Origin of Cytotoxicity and Surface Effects. *Small* **2009**, *5*, 701–708.
- Wang, L.; Jiang, X.; Ji, Y.; Bai, R.; Zhao, Y.; Wu, X.; Chen, C. Surface Chemistry of Gold Nanorods: Origin of Cell Membrane Damage and Cytotoxicity. *Nanoscale* **2013**, *5*, 8384–8391.
- Chen, C.-C.; Lin, Y.-P.; Wang, C.-W.; Tzeng, H.-C.; Wu, C.-H.; Chen, Y.-C.; Chen, C.-P.; Chen, L.-C.; Wu, Y.-C. DNA-Gold Nanorod Conjugates for Remote Control of Localized Gene Expression by near Infrared Irradiation. *J. Am. Chem. Soc.* **2006**, *128*, 3709–3715.
- Cobley, C. M.; Chen, J. Y.; Cho, E. C.; Wang, L. V.; Xia, Y. N. Gold Nanostructures: A Class of Multifunctional Materials for Biomedical Applications. *Chem. Soc. Rev.* **2011**, *40*, 44–56.
- Kah, J. C.; Chen, J.; Zubietta, A.; Hamad-Schifferli, K. Exploiting the Protein Corona around Gold Nanorods for Loading and Triggered Release. *ACS Nano* **2012**, *6*, 6730–6740.
- Cifuentes-Rius, A.; de Puig, H.; Kah, J. C.; Borros, S.; Hamad-Schifferli, K. Optimizing the Properties of the Protein Corona Surrounding Nanoparticles for Tuning Payload Release. *ACS Nano* **2013**, *7*, 10066–10074.
- Hühn, D.; Kantner, K.; Geidel, C.; Brandholt, S.; De Cock, I.; Soenen, S. J.; Rivera Gil, P.; Montenegro, J. M.; Braeckmans, K.; Mullen, K.; et al. Polymer-Coated Nanoparticles Interacting with Proteins and Cells: Focusing on the Sign of the Net Charge. *ACS Nano* **2013**, *7*, 3253–3263.
- Kah, J. C. Y.; Zubietta, A.; Saavedra, R. A.; Hamad-Schifferli, K. Stability of Gold Nanorods Passivated with Amphiphilic Ligands. *Langmuir* **2012**, *28*, 8834–8844.
- Domínguez-Medina, S.; Blankenburg, J.; Olson, J.; Landes, C. F.; Link, S. Adsorption of a Protein Monolayer Via Hydrophobic Interactions Prevents Nanoparticle Aggregation under Harsh Environmental Conditions. *ACS Sustainable Chem. Eng.* **2013**, *1*, 833–842.
- Gebauer, J. S.; Malissek, M.; Simon, S.; Knauer, S. K.; Maskos, M.; Stauber, R. H.; Peukert, W.; Treuel, L. Impact of the Nanoparticle-Protein Corona on Colloidal Stability and Protein Structure. *Langmuir* **2012**, *28*, 9673–9679.

38. Audouy, S.; Molema, G.; de Leij, L.; Hoekstra, D. Serum as a Modulator of Lipoplex-Mediated Gene Transfection: Dependence of Amphiphile, Cell Type and Complex Stability. *J. Gene Med.* **2000**, *2*, 465–476.
39. Verma, A.; Stellacci, F. Effect of Surface Properties on Nanoparticle-Cell Interactions. *Small* **2010**, *6*, 12–21.
40. Rauch, J.; Kolch, W.; Laurent, S.; Mahmoudi, M. Big Signals from Small Particles: Regulation of Cell Signaling Pathways by Nanoparticles. *Chem. Rev.* **2013**, *113*, 3391–3406.
41. Sahay, G.; Alakhova, D. Y.; Kabanov, A. V. Endocytosis of Nanomedicines. *J. Controlled Release* **2010**, *145*, 182–195.
42. Hinderliter, P. M.; Minard, K. R.; Orr, G.; Chrisler, W. B.; Thrall, B. D.; Pounds, J. G.; Teeguarden, J. G. ISDD: A Computational Model of Particle Sedimentation, Diffusion and Target Cell Dosimetry for *in Vitro* Toxicity Studies. *Part Fibre Toxicol.* **2010**, *7*, 36–56.
43. Cho, E. C.; Zhang, Q.; Xia, Y. N. The Effect of Sedimentation and Diffusion on Cellular Uptake of Gold Nanoparticles. *Nat. Nanotechnol.* **2011**, *6*, 385–391.
44. Epstein, J.; Kelly, C. E.; Lee, M. M.; Donahoe, P. K. Effect of *E. Coli* Endotoxin on Mammalian Cell Growth and Recombinant Protein Production. *In Vitro Cell. Dev. Biol.* **1990**, *26*, 1121–1122.
45. Hu, W.; Peng, C.; Lv, M.; Li, X.; Zhang, Y.; Chen, N.; Fan, C.; Huang, Q. Protein Corona-Mediated Mitigation of Cytotoxicity of Graphene Oxide. *ACS Nano* **2011**, *5*, 3693–3700.
46. Hawley-Nelson, P.; Ciccarone, V.; Moore, M. L. Transfection of Cultured Eukaryotic Cells Using Cationic Lipid Reagents. *Current Protocols in Molecular Biology*; Wiley: New York, 2008; Chapter 9, pp 9.4.1–9.4.17.
47. Schaeublin, N. M.; Braydich-Stolle, L. K.; Schrand, A. M.; Miller, J. M.; Hutchison, J.; Schlager, J. J.; Hussain, S. M. Surface Charge of Gold Nanoparticles Mediates Mechanism of Toxicity. *Nanoscale* **2011**, *3*, 410–420.
48. Czekay, R. P.; Wilkins-Port, C. E.; Higgins, S. P.; Freytag, J.; Overstreet, J. M.; Klein, R. M.; Higgins, C. E.; Samarakoon, R.; Higgins, P. J. PAI-1: An Integrator of Cell Signaling and Migration. *Int. J. Cell Biol.* **2011**, *2011*, 562481.
49. Aggarwal, B. B. Signalling Pathways of the TNF Superfamily: A Double-Edged Sword. *Nat. Rev. Immunol.* **2003**, *3*, 745–756.
50. Alberts, B.; Johnson, A.; Lewis, J.; Raff, M.; Roberts, K.; Walter, P. *Molecular Biology of the Cell*, 5th ed.; Garland Science: New York, 2008.
51. Sau, T. K.; Murphy, C. J. Seeded High Yield Synthesis of Short Au Nanorods in Aqueous Solution. *Langmuir* **2004**, *20*, 6414–6420.